Contribution from Lash Miller Chemistry Laboratory and Erindale College, University of Toronto, Toronto, Ontario, Canada

Optical Studies of the Genesis of Ligand-Free Cobalt and Rhodium Clusters: Relevance to Oxide- and Polymer-Bound Cobalt and Rhodium Clusters

GEOFFREY A. OZIN* and A. J. LEE HANLAN

Received November 9, 1978

The matrix aggregation reactions of cobalt and rhodium atoms to very small metal clusters are studied by optical spectroscopy in inert gas and methane supports by using a combination of metal concentration, matrix variation, temperature-dependent bulk, surface, and photodiffusion-nucleation, as well as cluster photofragmentation, techniques. Together with preliminary, spin-restricted, ground-state SCF–Xα–SW cluster molecular orbital calculations, the possibility of utilizing the electronic information derived from weakly perturbed, "ligand-free" metal clusters for characterizing the chemically extruded metal frameworks of discrete metal carbonyl cluster complexes bound to and perturbed by the anchoring sites of, for example, oxide, polymer, ligand silica, and zeolite supports is contemplated.

Introduction

With the growing interest in the catalytic properties of very small, uniquely graded, unimetallic (and bimetallic) particles, extruded from the well-defined metallic cores of discrete metal carbonyl cluster complexes and anchored to the active surface sites of functionalized organic polymers, phosphinated silicas, zeolites, or conventional oxide supports,[1] it is becoming increasingly evident that reliable methods need to be established to ascertain whether or not the original nuclearity of the cluster framework has been maintained throughout the process of going from the molecular state to the metallic state on the support. Supported metal clusters prepared in this way can be expected to lead to extremely narrow distributions of particle sizes in that critical size range which up to now has eluded systematic characterization.[1]

Once being in the reaction cycle of carbonyl cluster adsorption on a support, followed by vacuum thermal decarbonylation with subsequent oxidation or reduction, questions remain as to whether or not the surface species obtained has kept the original metal-cluster framework. Infrared data can in principle discern (a) whether the integrity of a very small particle has been retained, indicating low aggregation, (b) whether the zerovalent metal oxidation state has been altered, (c) whether the distribution of terminal and bridge carbonyl groups has been changed, and (d) whether conversion from a molecular-cluster framework to the metallic particle condition has ensued. Generally speaking, however, apart from a few isolated reports, cluster–surface interactions and the associated agglomeration processes remain uncharacterized.[1]

Considering the intensity of interest recently devoted to supported cobalt, rhodium, and iridium metal particle catalysts derived from, for example, $Co_2(CO)_8$, $Co_4(CO)_{12}$, $Rh_4(CO)_{12}$, $Rh_6(CO)_{16}$, and $Ir_4(CO)_{12}$ clusters and stably dispersed on various matrix supports and, in particular, to the proposal that the active sites consist of coordinatively unsaturated metal clusters comprising only a few atoms, we decided to pursue a systematic optical study of small cobalt and rhodium ligand-free clusters in order to learn about the size dependence of the electronic properties of these clusters in weakly interacting matrix supports. Comparisons with the same clusters perturbed by anchoring atoms or ligands on the surfaces of oxides, zeolites, ligand silicas, and functionalized polymers are anticipated to evolve from these studies.

Experimental Section

Monatomic Co and Rh vapors were generated by directly heating a 0.020 in. ribbon filament of the metal with ac in a furnace similar to that described previously.[37] The cobalt and rhodium (99.99%) were supplied by McKay, New York. Research grade Ar, Kr, Xe, and CH_4 (99.999%) were supplied by Matheson of Canada. The rate of Co and Rh atom deposition was continuously monitored with a quartz crystal microbalance.[38]

In the UV–visible experiments, matrices were deposited onto an NaCl optical window cooled to 10–12 K by means of an Air Products Displex closed-cycle helium refrigerator or to 4–6 K by an Air Products liquid helium transfer system. Ultraviolet–visible spectra were recorded on a standard Varian Techtron in the range 190–900 nm. Photolysis experiments employed an Oriel 1000-W Xenon lamp–Schoeffel monochromator assembly.

Cobalt Clusters. In addition to providing an insight into the electronic and mechanistic details of cobalt cluster formation, the study of few-atom cobalt clusters is also of interest from the point of view of their potential as methanation[2] and Fischer–Tropsch catalysts.[3] Various techniques, in addition to the usual metal salt reduction over a solid support, have recently been used for generating ultrafine cobalt particles. From the thermal decomposition of $Co_2(CO)_8$, dissolved in toluene in the presence of a surface-active agent, Papirer[4] found evidence for the formation of either well-defined spherical particles or irregular aggregates of cobalt, and Reike[5] reported the formation of highly reactive cobalt powders when ethereal or hydrocarbon solutions of cobalt halide salts were reduced with alkali metals. Gray and Frazier[6] impregnated poly(vinyl)pyridine microspheres with solutions of $Co_2(CO)_8$ which were subsequently photolyzed to generate either a cobalt subcarbonyl or cobalt cluster "polymer photocatalyst" which demonstrated impressive activity/selectivity patterns for olefin hydroformylation reactions. By use of a metal atom approach, Klabunde[7] formed various Co atom/toluene dispersions which, when warmed from −196 °C in the presence of carbon monoxide, led to the formation of $Co_2(CO)_8$, $Co_4(CO)_{12}$, $Co_6(CO)_{16}$, and higher unidentified cobalt carbonyl cluster complexes. In a somewhat similar manner, Wada[8] vaporized cobalt in the presence of a low pressure of helium gas (gas evaporation technique) onto a frozen solvent at −196 °C to produce dispersed cobalt particles.

Aside from Klabunde's[7] report, which suggests the possibility of small cobalt clusters in the $Co_2 \rightarrow Co_6$ range, these methods generally produce large aggregates of cobalt. By employment of the metal-atom matrix synthetic technique, whereby cobalt vapor is quantitatively condensed with various weakly interacting supports at 6–25 K, it has proven possible to identify electronic transitions attributed to Co_2 and Co_3 in the presence of those of atomic cobalt.

Atomic Cobalt. The optical spectrum of matrix-isolated cobalt atoms obtained at liquid helium temperatures (4.2 K) was first reported by Mann and Broida[9] in 1971. Our initial investigations of cobalt atom clustering-matrix reactions revealed that only on depositing cobalt at temperatures *below 10 K* was it possible to obtain optical spectra of atomic cobalt essentially free of absorbances attributed to dicobalt and higher clusters. In fact, as will be discussed later, this delicate temperature-dependent cobalt atom aggregation phenomenon proved to be the essential criterion for the formation and identification of higher cobalt clusters.

When cobalt atoms were deposited with Ar at high dilutions (Co/Ar $\simeq 1/10^4$) and at liquid helium temperatures (4.2–6 K), the optical spectrum shown in Figure 1 was obtained. For purposes of comparison, a stick representation of the free-atom gas-phase spectrum of cobalt[10] is included in Figure 1. The quality of the spectral data of the present study was superior to that of Mann and Broida,[9] but apart from some high-energy absorptions not observed by the latter, the two spectra were in good agreement, as the comparison in Table I indicates.

Taking into account the level ordering, selection rules, and oscillator strengths for the optical transitions of gaseous cobalt atoms, as

0020-1669/79/1318-1781$01.00/0

Table I. Optical Spectrum of Cobalt Atoms in Solid Argon at 4.2 K with Corresponding Free-Atom Transitions[a]

free atom (gas phase)		obsd in solid Ar			obsd in solid Ar			
nm	cm^{-1}	nm (4.2 K)	cm^{-1} (this study)	$\nu_M-\nu_G$, cm^{-1}	nm (4.2 K)	cm^{-1} (ref 22)	config	designation
352.7	28 346	348 w	28 735	389	348	28 735	$3d^74s4p$	$^4F^0_{9/2}$
347.4	28 777	339 m	29 498	721	337	29 673		$^4F^0_{7/2}$
346.6	28 845	335 m	29 850	1005	334	29 940		$^4G^0_{11/2}$
341.3	29 295	330 m	30 303	1008	330	30 303		$^4F^0_{7/2}$
		325 m	30 769	1474				
312.1	32 028	301 w	33 222	1194			$3d^84p$	$^4D^0_{7/2}$
308.3	32 431	295 sh	33 898	1467	299	33 444	$3d^84p$	$^4G^0_{11/2}$
304.4	32 842	292 m	34 246	1404	292	34 246		$^4F^0_{9/2}$
298.7	33 467	285 w	35 087	1620	284	35 211		$^4F_{7/2}$
252.1	39 649	252 ms	39 682	33	252	39 682	$3d^74s4p$	$^4D^0_{7/2}$
					250	40 000		
242.5	41 226	247 s	40 485	−741	245	40 816		$^4F^0_{9/2}$
240.7	41 529	239 s	41 841	312	242	41 322		$^4G^0_{11/2}$
					240	41 666		
238.5	41 918	236 s	42 372	454	238	42 016		$^4F^0_{7/2}$
236.5	42 269	234 s	42 735	466	234	42 735		$^4G^0_{9/2}$
230.9	43 295	228 w, sh	43 869	574	232	43 103		$^4F^0_{9/2}$
223.3	44 782	222 ms	45 045	263	222	45 045	$3d^85s$	$^4F^0_{9/2}$
213.3	46 872	214 w	46 729	−143			$3d^74s4p$	$^4D^0_{7/2}$
210.4	47 524	210 w	47 619	95			$3d^74s5s$	$^4F^0_{9/2}$
207.4	47 217	208 w	48 076	−141			$3d^74s4p$	$^4D^0_{7/2}$
197.0	50 741	200 w	50 000	−741			$3d^74s4p$	$^4D^0_{7/2}$

[a] Ground-state electronic configuration for cobalt is $3d^74s^2(^4F_{9/2})$.

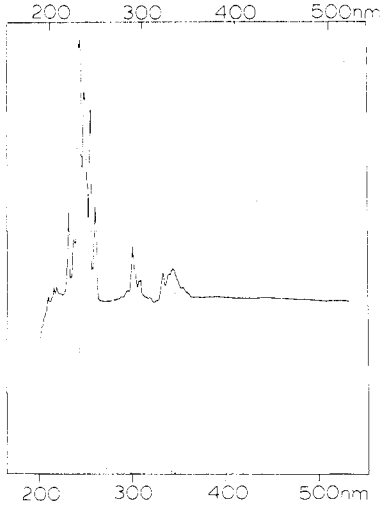

Figure 1. Optical spectrum of cobalt atoms isolated in solid Ar at 4.2–6 K, compared to the gas-phase atomic transitions of cobalt. The stick heights correspond roughly to reported oscillator strengths (AMCOR technique[10]).

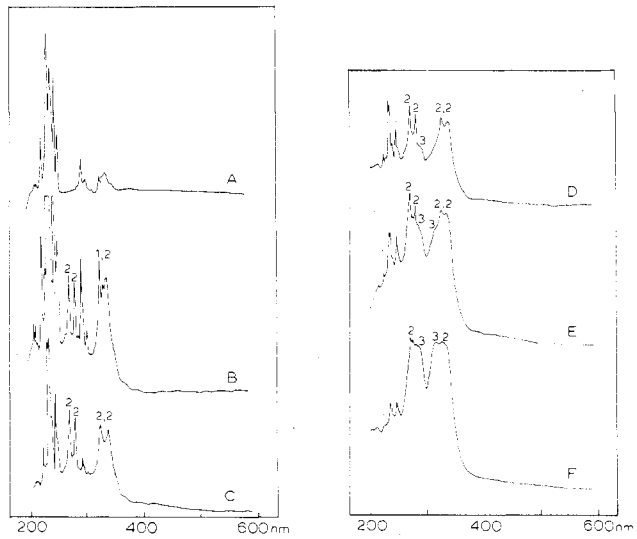

Figure 2. Ultraviolet–visible absorption spectra of Co/Ar ≃ $1/10^4$ mixtures deposited at (A) 4.2–6, (B) 10, (C) 13, (D) 15, (E) 20, and (F) 25 K, showing the progression from isolated Co atoms to Co/Co_2 to $Co/Co_2/Co_3$ mixtures.

documented by Moore,[11] a more accurate correlation of the matrix and gas-phase spectra can be obtained (AMCOR technique),[10] as given in Table I. Noteworthy is the general blue shift of the order of 30–1600 cm^{-1} on going from the gaseous atom to one entrapped in an argon cage. Such an energy shift is a general observation for matrix-isolated atoms.[9,12] The one-to-one correlation between matrix-phase and gas-phase atomic cobalt spectra indicates that under the vaporization, matrix temperature, and dilution conditions used, atomic cobalt was the primary species formed and isolated in solid argon.

Dicobalt and Tricobalt. In 1964 Kant and Strauss[13] observed the mass spectrum of Co atoms and Co_2 in equilibrium with liquid cobalt and reported a bond dissociation energy for dicobalt of $D_e = 39 \pm 6$ kcal/mol. Cooper, Clarke, and Hare[14] made use of this dicobalt bond energy data in an EHMO study of Co_2 (as well as other first-row transition-metal diatomic molecules) and concluded that partially filled 3d orbitals contributed to the metal–metal bonding (our SCF–Xα–SW calculations support this view).[17] Other than these studies no other information for Co_2 or higher cobalt clusters has appeared.

In this study various approaches were adopted in a search for dicobalt and higher cluster UV–visible absorption data. Evidence for cobalt-atom aggregation at the few-atom extreme first came from a comparison of the observed optical spectra for Co/Ar ≃ $1/10^4$ mixtures recorded at 4–6 and 10–12 K (Figure 2A,B). A difference of approximately 4–6 K was sufficient to cause the appearance of an entirely new set of optical absorptions in the regions 320–340 and 270–280 nm (Figure 2A,B).

To assist in the assignment of electronic transitions of Co_2 and other small cobalt clusters, the intensities of the various bands were examined with respect to their dependence on the cobalt concentration, matrix material, and deposition temperature along with their behavior during selective matrix photolysis. The results revealed the presence of a Co_2 species and probably a Co_3 species as well as higher stages of cobalt cluster formation.

Metal Concentration Studies. Unlike other transition-metal atom/dimer studies,[15] increasing the metal concentration over a wide range of cobalt–argon depositions did not result in a continuous increase in the intensities of those spectral features suspected for Co_2, accompanied by a decrease in the atomic absorptions. Instead, the overall intensities of all bands were observed to decrease with increasing metal concentration, even when beginning with very high Co/Ar dispersions. This behavior made it difficult to obtain meaningful metal concentration data for the purposes of identifying cluster size.[16] The general trend, however, was a growth of the optical transitions at 270

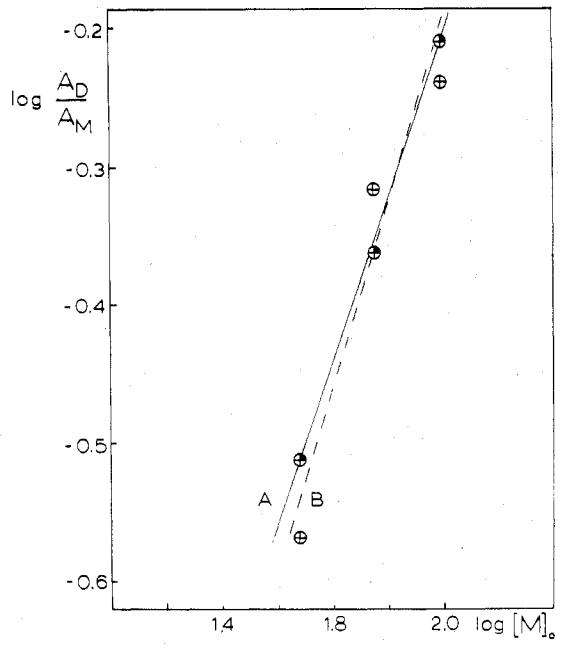

Figure 3. A log–log plot of the ratio of the absorbances of (A) the 270-nm band and (B) the 280-nm band attributed to Co_2 to that of the Co atomic resonance band at 246-nm as a function of Co deposition rate at constant Ar deposition rate.

and 280 nm *relative* to those of the identified atomic transitions. Figure 3 shows the results of a partial concentration study of cobalt atoms in argon. For each of the observed bands at 270 and 280 nm, the log of the ratio of their absorbance to that of the absorbance of the atomic transition at 246 nm was plotted against the log of the total metal concentration, resulting in two straight lines of slopes of roughly 0.85 and 0.90. These gradients, very close to unity, are in accord with the cluster-model kinetic theory of Moskovits and Hulse,[16] supporting the assignment of the 270- and 280-nm bands to electronic transitions of diatomic cobalt. Quantitative analysis of the other new spectral features (in the 320–340-nm region) in this same manner was not possible due to their overlap with atomic absorptions. The observed decrease in intensities of both atomic and diatomic absorptions as metal concentration was increased suggested that even at relatively low metal concentrations ($1/10^3$ to $1/10^4$), higher cobalt clusters than Co_2 were being formed but with absorptions either too weak to observe or else hidden under existing atomic and diatomic bands. This would also account for the seemingly low growth of diatomic transitions with increasing metal concentration and the difficulty of obtaining quantitative data in the manner described by Moskovits and Hulse.[16]

Experiments in Ar, Kr, Xe, and CH_4. Using ratios of Co/matrix $\simeq 1/10^4$ and deposition temperatures of 10–12 K, we obtained optical spectra in Ar, Kr, Xe, and CH_4, and these are compared in Figure 4 and Table II. When we moved to the more rigid matrix materials, the absorbances attributed to atomic cobalt (Table I) increased in intensity, while the bands at 270 and 280 nm monotonically decreased, accompanied by spectral changes in the 320–340-nm region. The intensity behavior of the spectral features on changing to matrix materials expected to impede dimer formation suggests assignment of the 270- and 280-nm bands to electronic transitions of dicobalt, as previously indicated by the metal concentration study, and supports the contention of an overlap of Co atomic transitions with those of Co_2 or possibly higher cobalt clusters in the 320–340-nm region.

Variation of the Deposition Temperature. The effect of deposition temperature on the tendency of cobalt atoms to form small clusters was most revealing in terms of optical assignments as well as activation energy considerations. When cobalt atoms were deposited under dilute metal/argon matrix conditions for a series of selected temperatures ranging from 4.2–6 to 25 K (Figure 2A–F), dramatic spectral changes ensued that could be attributed to the early stages of cobalt cluster growth. Between 4.2–6 and 10 K (Figure 2A,B) the first stage of cobalt atom aggregation was apparent with new bands present at 270 and 280 nm and relative intensity changes in the 320–340-nm region at the higher temperature, in accordance with the concentration and matrix-variation studies which pinpointed the growth of the Co_2 species.

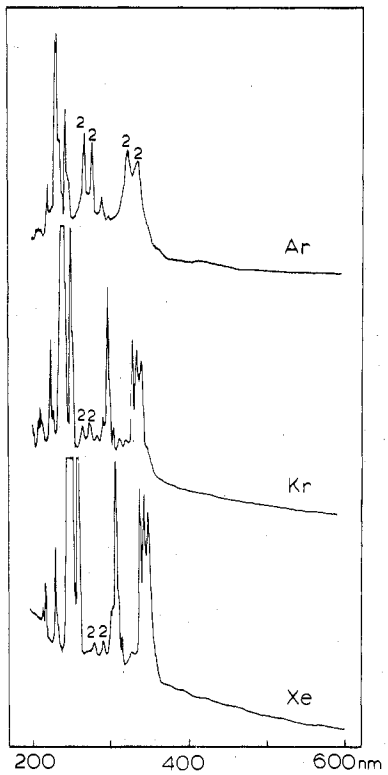

Figure 4. Correlation of UV–visible spectra of Co atoms and Co_2 molecules coisolated in Ar, Kr, and Xe matrices under identical conditions of temperature, gas, and metal-deposition rates.

Table II. Optical Spectra of Cobalt Atoms in Solid Ar, Kr, Xe, and CH_4 at 10–12 K Compared to the Gas-Phase Atomic Transitions (nm)

free atom (gas phase)	argon	krypton	xenon	methane
352.7	348			
347.4	339	341	349	340
346.6	335	335	344	335
341.3	325	329	338	
312.1	301	306	314	310
308.3	295	302	310	304
304.4	292	298	306	300
298.7	285	291	299	
252.1	249	253	258	253
242.5	246	250		
240.7	238	240	248	243
238.5	235	237	247	241
236.5	232	235		236
230.9	228			232
223.3	222	226	229	227
213.3	214			
210.4	210	211	217	213
207.4	208	209	207	
197.0	200			203

On progressing to approximately 13 K (Figure 2C), we observed that there was a marked decrease in the cobalt atomic resonance lines relative to the new spectral features at 340, 320, 280, and 270 nm. These effects were even more pronounced at 15 and 20 K (Figure 2D,E); particularly significant at these higher temperatures was evidence for a second stage of cobalt clustering, as seen by a new set of broad optical absorptions at roughly 287 and 316 nm. These new bands displayed different growth/decay characteristics than those associated with atomic Co and Co_2. The presence of this third cobalt species was most evident from the highest temperature deposition (25 K, Figure 2F). Under these conditions the most intense cobalt atom resonance bands, around 250 nm, had essentially decayed to zero while almost equal absorbances of dicobalt and the third cobalt species, partially overlapping in the 270–300- and 320–350-nm regions, dominated the optical spectrum. The unique growth behavior of this third cobalt species following the appearance of Co_2 suggested that

Table III

Optical Transitions (nm) of Dicobalt Observed in Solid Ar, Kr, Xe, and CH_4 at 10–12 K

Ar[c]	Kr	Xe	CH_4
442	*a*	*a*	445
418	*a*	*a*	410/420
340[b]	338[b]	*d*	*d*
320[b]	320[b]	*d*	*d*
280	284	290	283
270	274	279	274

Optical Spectrum of Tricobalt Observed in Argon at 20–25 K (nm): 400–480, 316, 287

[a] Too weak to observe. [b] Observed after warm deposition (15–20 K). [c] Matrix photolysis experiments suggest the presence of a Co_2 absorption in the atomic region around 290 nm. [d] Band overlap problems.

a tentative assignment to molecular Co_3 was reasonable.

Matrix Photolysis Experiments. The matrix photolysis of cobalt atoms and dimers proved to be unrewarding in the search for cluster species higher than Co_2 or Co_3. The results, however, did provide further support for the assignment of optical transitions of Co_2 and Co_3 made on the basis of metal concentration, matrix material, and deposition temperature studies. On the basis of the results of other reported atom/cluster photolysis studies,[15d,33a,b] it was expected that irradiation into certain cobalt atomic resonance lines might lead to cobalt atom photodiffusion, i.e., growth of diatomic and higher cluster absorptions with concomitant decay of cobalt atomic resonance lines (see Rh/Rh_2 cryophotochemical reactions described later). Instead, the result of irradiation into the 292-nm band of atomic cobalt was total *loss* of the 270- and 280-nm dicobalt absorptions accompanied by a *slight increase* in the measured intensities of the atomic transitions, just opposite to the expected behavior. Such unanticipated spectral changes might be explained by the presence of an unsuspected Co_2 absorption hidden under the 292-nm atomic Co transition. However, *decay* of the diatomic bands did also occur on direct irradiation either of the 270- or 280-nm Co_2 bands, as expected, or in the 320–350-nm region previously established to contain an overlap of atomic, diatomic, and triatomic cobalt. An overlap of atomic Co and Co_2 bands in these two regions would explain the unsuccessful attempts to generate dicobalt through photoaggregation of the atoms, since simultaneous irradiation of atomic and diatomic resonance transitions might be expected to result in competition between photoaggregation of atoms to dimers and photodissociation of dimers to atoms (see Rh/Rh_2 later).

For these kinds of photolysis experiments, where subtle intensity changes of bands may occur, strongly absorbing samples are desired. Under such conditions broad weak features were observed in the cobalt optical spectrum around 418 and 442 nm. Upon 292-nm irradiation, these two low-energy bands were observed to lose some intensity, concomitant with the decay of the 270- and 280-nm bands, pointing to the existence of Co_2 transitions in the 400–450-nm region. That these low-energy bands did not decay completely to zero on photolysis, as do the other Co_2 bands, leads one to postulate that higher clusters, perhaps Co_3, also absorb in the low-energy region.

Taking all evidence into consideration, it can be concluded that three distinct cobalt species can be formed, the optical characteristics of which permit a tentative assignment to Co, Co_2, and Co_3 as presented in Tables I–III.

SCF–Xα–SW Molecular Orbital Calculations for Co_2 and Co_3. To complement these data we have calculated the electronic energy levels for linear Co_2 and Co_3 by the SCF–Xα–SW molecular orbital procedure.[17] A brief mention of these computations will be referred to here. Preliminary spin-unrestricted calculations of the optical spectrum for dicobalt were found to agree quite well with the observed spectra as seen by reference to Table IV. Partial wave analyses showed that the valence s band overlaps the d band in Co_2 (as well as in Co_3 and in Co metal itself), resulting in significant 4s character in the formally 3d-derived $1\sigma_g$ orbital and 3d character in the formally 4s-derived $2\sigma_g$ orbital, leading to the conclusion that the metal–metal bond in Co_2 has a significant d contribution.[43]

Calculations for an assumed linear Co_3 molecule (other geometries will be considered in a later publication)[17] predicted a number of allowed electronic transitions in three basic regions of the spectrum (390–470, 350, and 290–330 nm), which can be roughly correlated with the broad optical absorptions observed for tricobalt (Table IV). Input parameters used in the Co_2, Co_3 calculation are given in Table IV. From data of this type one can begin to appreciate the early development of the dsp orbital structure of larger cobalt clusters and the genesis of the band picture and optical properties of cobalt metal itself. Of significance here is the already close approach of the absorption spectrum of Co_3 (316, 287 nm) to the proposed optical transitions reported for massive Co particles and bulk Co films which show maxima around 250–325 nm.[18] Full details of these Xα calculations will be reported in a separate paper.[17,43]

Table IV. Observed and Calculated (SCF–Xα–SW–MO) Optical Spectra of Dicobalt, Co_2, and Tricobalt, Co_3 (in nm)[17]

obsd in argon[h]	calcd[a,d]	tentative assignts[g]
	Co_2[b] Spectrum	
442[f]	490	$2\sigma_g^+ \rightarrow 2\sigma_u^+$
418[f]	430	$1\pi_g \rightarrow 2\pi_u$
340[e]	355	$2\sigma_g^+ \rightarrow 2\pi_u$
320	305	$1\sigma_g^+ \rightarrow 2\sigma_u^+$
280[e]	252	$1\pi_u \rightarrow 3\sigma_g^+$
270	247	$1\sigma_g^+ \rightarrow 2\pi_u$
	Co_3[c] Spectrum	
	468	$2\sigma_u^+ \rightarrow 4\sigma_g^+$
	411	$1\sigma_g^+ \rightarrow 2\sigma_u^+$
400–480[f]	396	$1\pi_u \rightarrow 4\sigma_g^+$
	392	$2\sigma_g^+ \rightarrow 2\pi_u$
	362	$1\sigma_u^+ \rightarrow 4\sigma_g^+$
316	352	$2\sigma_u^+ \rightarrow 5\sigma_g^+$
	329	$1\pi_g \rightarrow 2\pi_u$
287	310	$1\pi_u \rightarrow 5\sigma_g^+$
	289	$1\sigma_u^+ \rightarrow 5\sigma_g^+$
	228	$1\sigma_g^+ \rightarrow 2\pi_u$

[a] As a starting point, the sum of the covalent radii, 2.32 Å, was employed in these calculations. [b] Calculated Co_2 ground-state configuration $(1\sigma_g)^2(1\pi_u)^4(1\delta_g)^4(2\sigma_g)^2(1\delta_u)^4(1\pi_g)^2$. [c] Calculated Co_3 ground-state configuration $(1\sigma_g)^2(1\pi_g)^4(1\sigma_u)^2(1\delta_g)^4(2\sigma_g)^2(1\pi_u)^4(2\delta_g)^4(2\sigma_u)$ with ambiguity regarding HOMO which could be $(2\pi_g)$ or $(3\sigma_g)$. [d] Preliminary values for sphere radii obtained from spin-restricted ground-state transition energies with $\alpha = 0.71018$ (species, Bohr, Å): Co_2 (outer sphere), 4.95803, 2.62; Co_2 (Co sphere), 2.76590, 1.46; Co_3 (outer sphere), 7.14982, 3.78; Co_3 (central Co sphere), 2.57370, 1.36; Co_3 (outer Co Sphere) 2.76556, 1.46. Note that the Co spheres overlap in both Co_2 and Co_3 calculations but that the Norman prescription was not strictly adhered to. However, the sphere overlaps used differ by only roughly 5% from the Norman prescription,[27] and this is expected to have only a minimal effect on the calculated ground-state transition energies. Detailed spin-unrestricted transition-state calculations will be reported later on.[17] [e] Narrow band, continuous photoexcitation in these bands causes photobleaching of all of the dicobalt absorptions. [f] Region of extremely weak absorptions associated with Co_2, Co_3, and possibly higher Co_n clusters. [g] See ref 43. [h] Matrix photolysis experiments suggest that a weak Co_2 absorption overlaps with a Co atomic line around 290 nm.

Rhodium Clusters. The chemistry of rhodium vapor has been explored to a limited extent in studies of the cocondensation reactions with dinitrogen,[19] carbon monoxide[20] and dioxygen.[21,22] The results of these studies have indicated the pronounced tendency for Rh to form binuclear and trinuclear complexes. The facile matrix surface diffusion and aggregation properties of Rh atoms were first recognized in a series of Rh/N_2 cocondensation experiments by the identification of $Rh_2(N_2)_x$ species (where x was thought to most likely be 8).[19] Clearer evidence of the clustering processes involved was deduced from quantitative Rh atom concentration experiments in CO matrices where both $Rh(CO)_4$ and $Rh_2(CO)_8$ were synthesized and characterized.[20] The ease of formation of these binuclear $Rh_2(N_2)_x$[19] and $Rh_2(CO)_8$[20] complexes prompted a preliminary investigation of the fate of Rh atoms when cocondensed with inert-gas matrices, from which some Rh_2 optical transitions were identified; however, higher Rh_n cluster absorptions were not recognized at that time.[22]

Additional motivation for seeking new experimental routes to small rhodium clusters of known composition relates to the industrial use of supported rhodium catalysts in a variety of hydrocarbon oxidation reactions[23] and in automobile exhaust antipollution systems.[24] Recent insight into the possible catalytic importance of few-atom Rh clusters

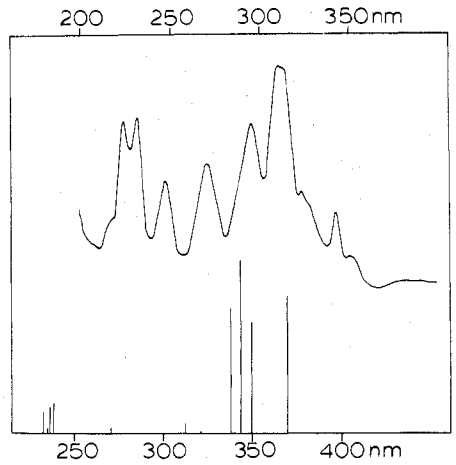

Figure 5. Optical spectrum of Rh atoms isolated in solid Ar at 10–12 K, compared to the gas-phase atomic transitions of Rh.[22] The stick heights correspond to reported oscillator strengths[10] (AMCOR technique).

was first obtained by Collman[1c] from the reaction of rhodium carbonyl clusters with phosphinated polystyrene to afford polymer-$[C_6H_4PPh_2]_nRh_4(CO)_{12-n}$ and polymer-$[C_6H_4PPh_2]_nRh_6(CO)_{16-n}$. Aerial oxidation of these clusters led to the loss of ν(CO), and subsequent treatment with hydrogen produced what was believed to be *active metal particles consisting of four and six rhodium atoms*, respectively. The substance derived from $Rh_6(CO)_{16}$ was found to catalyze the hydrogenation of arenes at 25 °C in 1 atm of H_2, while that derived from $Rh_4(CO)_{12}$ exhibited a lower activity. Since this discovery, a number of other spectroscopic–catalytic studies involving the anchoring of $Rh_4(CO)_{12}$ and $Rh_6(CO)_{16}$ (as well as the iridium analogues) clusters to functionalized polymers, ligand silicas, and conventional oxide supports[1] have generally reenforced the idea that ligand dissociation from immobilized molecular clusters can lead to the metallic state in which the integrity of the cluster core has been retained. Significantly, the UV PES for the metal valence levels of clusters like $Rh_6(CO)_{16}$[1b] already show many similarities to those of the corresponding bulk metal, indicating that possibly as few as six rhodium atoms are required to simulate the major electronic features of rhodium metal itself. (Incidentally, this proposal is in line with recent optical[15d,33c,39,40] and theoretical[25] studies of Ag_n where n = 1–6.) This and other evidence for the formation and catalytic activity of discrete, few-atom metal clusters of rhodium[26] encouraged a further investigation of the clustering processes and optical properties of rhodium by the metal-atom matrix synthetic technique.

Atomic and Diatomic Rhodium. In our earlier study of Rh/inert gas cocondensation experiments, the optical transitions of atomic and diatomic rhodium were identified via metal concentration and matrix-variation techniques.[22] A typical Rh/Ar $\simeq 1/10^4$ spectrum which correlates the gas-phase and matrix atomic spectra of rhodium is shown in Figure 5, while spectra of concentration experiments such as those shown in Figure 6 allowed the identification of Rh_2 bands at 352, 344, 325, 317, and 312 nm, although atomic overlap problems precluded a definitive assignment of the 312–325-nm region.[22]

Matrix Photolysis Experiments. Rhodium atom photoaggregation and Rh_2 photodissociation experiments, to be described, considerably strengthen the conclusions drawn from the Rh concentration and matrix-variation experiments for the assignments of atomic and diatomic Rh transitions.[22] Furthermore, under the more controlled experimental conditions used, *new bands could be identified* with behavior which could also be associated with molecular dirhodium.

Starting with highly absorbing samples of atomic and diatomic Rh (Figure 7), so that subtle intensity changes on irradiation could best be observed, new weak bands were noticed for the first time in the 400- and 450-nm region. Absorptions of such low energy had not been observed for gas-phase atomic rhodium,[11] and so it was suspected that these new features could be associated with very weak transitions of dirhodium.

Photoexcitation into the strong electronic absorption of Rh_2 at 344 nm for 1 h (Rh/Ar $\simeq 1/10^3$) resulted in a remarkable *decrease* in the intensity of that band, accompanied by intensity loss in each of the distinct bands assigned to Rh_2 (Figure 7B). Measurement of the

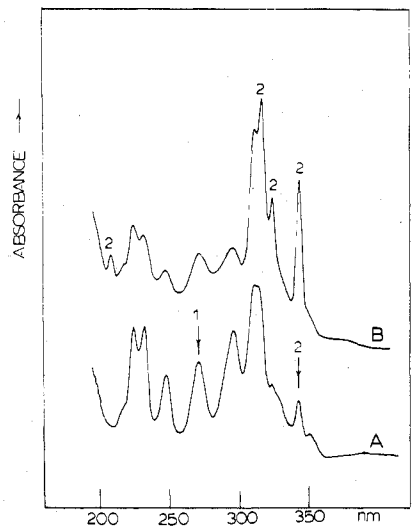

Figure 6. UV–visible spectrum of atomic Rh isolated in solid Ar at 10–12 K showing the effects of increasing the Rh/Ar ratio from roughly $1/10^4$ to $1/10^3$ (A to B).[22]

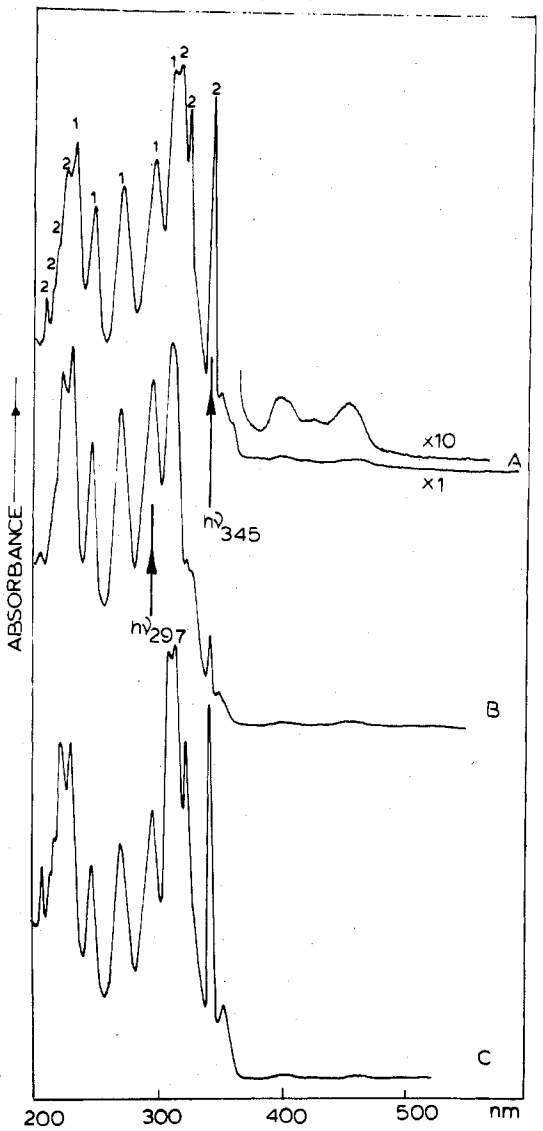

Figure 7. UV–visible spectrum of (A) Rh atoms and Rh_2 molecules at 10–12 K in solid Ar, (B) after 1-h photolysis at 345 nm showing the decay of Rh_2 and slight growth of Rh atoms, and (C) after 1-h photolysis at 297 nm showing the return growth of Rh_2 and decrease of Rh atoms.

Table V. Complete Optical Spectrum of Rh_2[a] Compared with the Calculated (SCF-Xα-SW-MO) Spectrum (in nm)

obsd in argon	calcd[27,43]	tentative assignt
460	461	$2\sigma_g^+ \rightarrow 2\sigma_u^+$
400	410	$1\sigma_g^+ \rightarrow 1\sigma_u^+$
352		
344	397	$1\pi_g \rightarrow 2\sigma_u^+$
325	395	$2\sigma_g^+ \rightarrow 2\pi_u$
317	336	$1\pi_g \rightarrow 2\pi_u$
312		
297	287	$1\delta_g \rightarrow 2\pi_u$
223		
217		
213	254	$1\delta_g \rightarrow 2\pi_u$
208		

[a] Observed in solid argon at 10–12 K.

atomic Rh bands revealed a slight *increase* in their intensities. Especially interesting was the high-energy 200–225-nm region, where under the high-intensity conditions of the spectrum before irradiation (Figure 7A), features could be observed at 223, 217, 213, and 208 nm. After the irradiation at 344 nm, the 217-, 213-, and 208-nm bands almost completely disappeared while the relative intensity of the 223-nm band with respect to the 233-nm atomic band changed, all concomitant with the decay of the observed diatomic, Rh_2, bands.

When the excitation energy was changed to correspond to that of the Rh atomic resonance band at 297 nm, a 1-h irradiation resulted in photodiffusion of atoms leading to aggregation and formation of Rh_2. This is illustrated in Figure 7C *by the return of the intensity of all bands associated with Rh_2 and a slight decrease in intensity of the atomic transitions*. It was also observed that the high-energy features at 223, 217, 213, and 208 nm experienced an increase in intensity. The parallel intensity behavior of this latter group of bands with those previously assigned to Rh_2[22] (Table V) suggested that they should also be assigned to electronic transitions of Rh_2. Figure 8 displays graphically the relative intensity changes of the three Rh atomic transitions at 297, 276, and 245 nm and that of Rh_2 at 344 nm, which took place during a series of irradiations at various wavelengths. The graph illustrates the slight relative increase in the intensity of the atomic bands that occurred on irradiation of the diatomic 344-nm band while the Rh_2 band decreased, representative of photodissociation of the dimer as a possible matrix photochemical pathway. A slight decrease in intensity of the atomic bands accompanied the increased diatomic concentration upon irradiation of the atomic 297-nm feature. The parallel intensity behavior displayed by the group of three Rh atomic absorptions, as illustrated in Figure 8, was quite different from the behavior of the 344-nm band and supports the existence of transitions belonging to two independent metal species, Rh and Rh_2.

Therefore, as a result of the selective UV irradiation experiments of the Rh and Rh_2 species, further evidence was obtained toward the identification of spectral features appropriate to either Rh or Rh_2. Furthermore, new bands were identified and associated with diatomic Rh_2 such that a more complete compilation of the ultraviolet absorption spectrum of molecular dirhodium is now available (Table V).

SCF–Xα–SW Molecular Orbital Calculations for Rh_2. On the basis of our initial observation of electronic spectral data for a molecular dirhodium species, Norman and Kolari[27] have performed some preliminary ground-state spin-restricted and spin-unrestricted Xα calculations for the Rh_2 molecule. Figure 9 displays their calculated valence energy levels for Rh_2 using a bond length of 2.39 Å. Owing to the crowding of MO levels around the Fermi level, the SCF–Xα–SW results indicated that dimerization of the d^8s^1 rhodium atom results in a redistribution of s and d electrons to give a final $d^{17}s^1$ $((2\sigma_g)^1(1\pi_g)^2(1\sigma_u)^1)$ configuration. A comparison of the calculated and observed transitions of Rh_2 is given in Table V and although the correlation is not exact, Norman's[27] results have predicted bands for Rh_2 in *three* main absorption regions, in accord with our observations.[43]

Referring then to Figure 9, it might be expected that transitions involving removal of electrons from the bonding $2\sigma_g$ (sd_z^2) orbital or placement of electrons into the antibonding $2\sigma_u$ (sp_z) level could represent dissociative states for matrix-entrapped Rh_2. From the assignments in Table V it can be seen that the observed 460-, 344-, and 325-nm optical excitations of Rh_2 could possibly all be assigned to dissociative transitions; *in practice, irradiation into the 344-nm Rh_2 band did indeed lead to Rh_2 dissociation.*[44]

The preliminary results of Norman's calculations therefore strengthen the assignments of the observed electronic transitions of Rh_2 and suggest that depletion of the dimer upon 344-nm excitation can, at least partly, be attributed to its photodissociation.

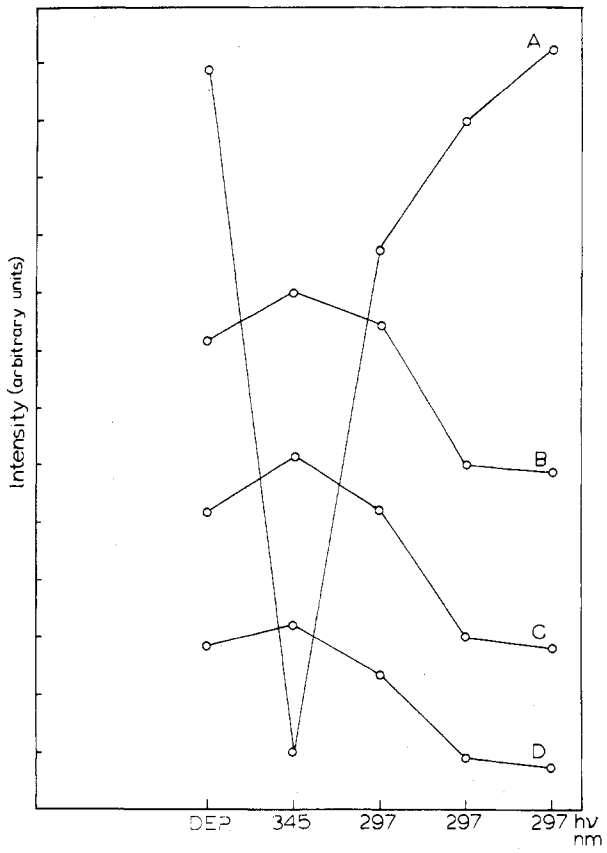

Figure 8. Graphical representation of the intensity changes which occurred in (A) the 344-nm Rh_2 band and in the Rh atomic bands at (B) 297, (C) 276, and (D) 245 nm during a consecutive series of irradiations of a Rh/Ar ≃ $1/10^3$ matrix.

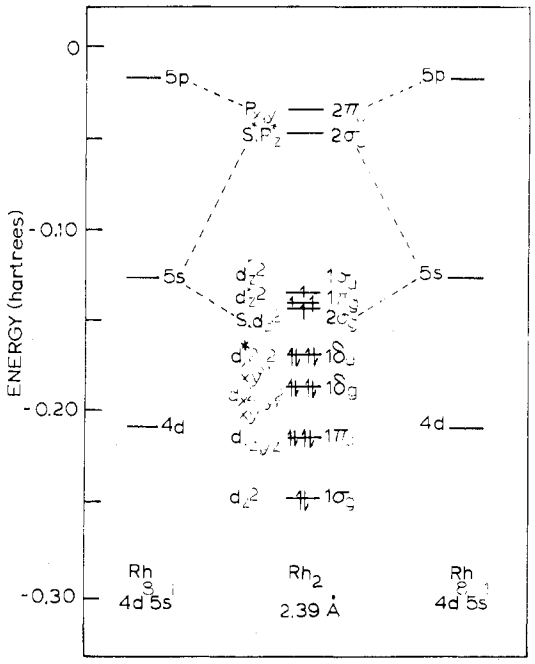

Figure 9. Spin-restricted valence energy levels for Rh and Rh_2, calculated by using SCF–Xα–SW molecular orbital theory (taken from ref 27).

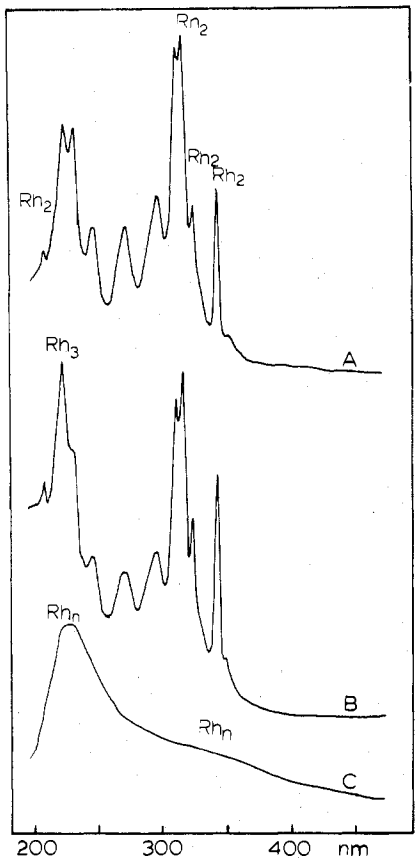

Figure 10. Optical spectra of Rh in solid Ar at (A) Rh/Ar $\simeq 1/10^3$, (B) Rh/Ar $\simeq 1/10^2$, deposited at 10–12 K, and (C) Rh/Ar $\simeq 1/10^2$, deposited at 25 K.

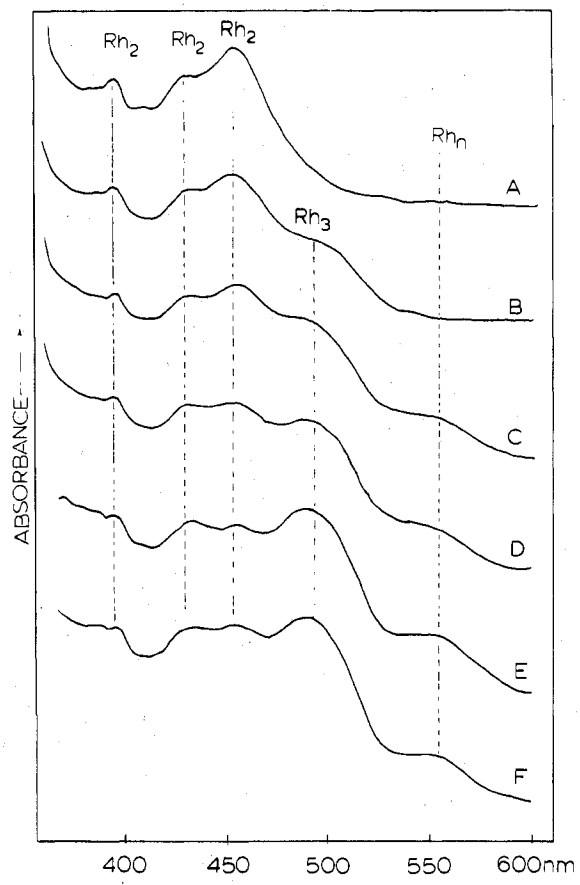

Figure 11. Optical spectra of Rh in solid Ar at ratios of Rh/Ar $\simeq 1/10^3$ showing the changes which occurred in the 400–500-nm range (illustrating the growth of a possible Rh_3 species at ~490 nm) (A) on deposition and after 45 min total photolysis at (B) 290, (C) 270, (D) 297, (E) 297, and (F) 345 nm.

Evidence for Higher Rhodium Clusters. In contrast to some of the other transition metals such as Cr, Ni, Co, Mo, Ag, or Cu,[15] for which electronic transitions assignable to trimer and higher cluster species have been found, no definite assignments could be made in the case of rhodium. There were, however, several pieces of evidence indicating that Rh_3 or higher Rh_n clusters were being formed, but with weak absorptions that either were difficult to detect or were hidden under the more intense Rh atomic and Rh_2 diatomic transitions.

Under conditions of very high metal concentration, Rh/Ar $\simeq 1/10^2$ to 1/10 broad background absorptions became noticeable in the 300-nm region. In Figure 10, examples of low and high metal concentration are compared, illustrating the difference in spectral baselines, which strongly suggests the presence of underlying features in the high-metal-concentration sample, possibly due to higher Rh_n cluster species. These broad background absorptions encompass most of the ultraviolet spectral range of both Rh and Rh_2 and thereby hindered identification of higher cluster absorptions.

In the course of studying Rh/Rh_2 formation, intensity variations of bands in the 220–230-nm region were also observed. The band at roughly 223 nm was often seen to grow in intensity in a manner that did not correlate with the observed growth of other Rh_2 bands, especially under conditions of high metal concentration. By use of warm deposition conditions (which, as already described, provided the most efficient way of identifying Co_n clusters), a broad band peaking at roughly 225 nm was observed to dominate the high-energy region with a weak broad absorption covering the 300–400-nm region; both atomic and diatomic transitions were completely absent. Some of the changes that occurred in this high-energy region are shown in Figure 10. The variation in the band shape in the 225-nm region under high-metal-concentration conditions may be indicative of the growth of a new Rh_n species, while the broad band obtained from the warm deposition may already represent aggregation beyond the few-atom level, approaching that of bulk rhodium of colloidal dimensions.

More convincing evidence for a specific band assignable to a Rh_3 species was observed in the low-energy 400–500-nm region. As previously mentioned, at very high metal concentrations, where large amounts of diatomic rhodium were present, weak low-energy bands were observed at approximately 400 and 460 nm, possibly associated with Rh_2. During the course of irradiation into either atomic or diatomic rhodium absorptions, a new band around 490 nm was observed to grow in (Figure 11). The growth of this band, seemingly independent of the excitation energy, may be explained by the formation of a Rh_3 species from Scheme I, where $Rh^\dagger$ and $Rh_2^\dagger$ represent photomobile rhodium atoms and rhodium dimers respectively.[15d]

Scheme I

$$Rh \rightarrow Rh^\dagger \quad \text{atomic excitation}$$

$$\left.\begin{array}{l} Rh_2 \rightarrow 2Rh^\dagger \\ \text{or} \\ Rh_2 \rightarrow Rh_2^\dagger \end{array}\right\} \text{diatomic excitation}$$

$$\left.\begin{array}{l} Rh^\dagger + Rh_2 \rightarrow Rh_3 \\ Rh_2^\dagger + Rh \rightarrow Rh_3 \end{array}\right\} \text{photoaggregation}$$

"Anomalous" Rh/Rh_2 Matrix Photolysis Behavior: Additional Evidence for Higher Rh_n Clusters. High Rh concentration experiments (Rh/Ar $\simeq 1/10^2$) employing Rh 297-nm photoexcitation yielded spectral intensity variations which were strikingly distinct from those observed under low-Rh-concentration conditions (Rh/Ar $\simeq 1/10^4$–$1/10^3$). For three consecutive 297-nm, 30-min irradiations, the 344-nm Rh_2 band was observed to decrease, increase, and then decrease again in intensity, with corresponding but *opposite* behavior of the monitored atomic transitions (297, 276, and 245 nm). These observations are in contrast to those of the low-metal-concentration experiments where 297-nm excitation was never observed to result in a decrease in the intensity of Rh_2 transitions. Such "anomalous" spectral behavior seems to be best interpreted in terms of a postulated Rh_2 component, coincident with or close in energy to the strong Rh 297-nm atomic absorption. Only in high-metal-concentration matrices did this weak Rh_2 component make its presence felt, passing unnoticed

Scheme II

i $Rh \xrightarrow[297\ nm]{k_1} Rh^{\dagger}$ photomobile Rh atom; decay route of Rh

ii $Rh_2 \xrightarrow[297\ nm]{k_2} 2Rh^{\dagger}$ photodissociation of Rh_2 and generation of photomobile Rh atoms; decay route of Rh_2

iii $Rh^{\dagger} + Rh \xrightarrow{k_3} Rh_2$ growth route of Rh_2; decay route of Rh

iv $Rh^{\dagger} + Rh_2 \xrightarrow{k_4} Rh_3$ decay route of Rh and Rh_2 causing gradual overall loss of Rh and Rh_2 bands; growth of Rh_3

in the low-Rh-concentration experiments.

We would therefore like to propose that photoexcitation into the 297-nm Rh/Rh_2-overlap region simultaneously initiates a sequence of time- and concentration-dependent photoaggregation/photodissociation events, approximately represented by Scheme II. From these reactions the origin of the alternate growth/decay characteristics of Rh_2 bands during photoexcitation of the 297-nm Rh/Rh_2-overlap region can be visualized and is expected to be dependent on the $[Rh]/[Rh_2]$ concentration ratio and the relative values of the rate constants k_1, k_2, k_3, and k_4 where

$$d[Rh_2]/dt = -k_2[Rh_2] + k_3[Rh^{\dagger}][Rh] - k_4[Rh^{\dagger}][Rh_2]$$

The concentration of photomobile rhodium atoms $[Rh^{\dagger}]$ is some complicated function of the excitation intensity and energy-transfer characteristics of 297-nm electronically excited Rh* and Rh_2*.

Similar arguments can be devised for a proposed Rh/Rh_3 overlap in the 297-nm region where events of the sort

$$Rh_3 \xrightarrow[297\ nm]{h\nu} Rh_2 + Rh$$ photodissociation step for Rh_3

could be considered. Clearly the observed data cannot eliminate this as an alternative explanation.

Although intended only to be qualitative, the above reaction schemes provide an entirely consistent set of photoevents to account for the anomalous spectral behavior observed under high-Rh-concentration conditions, that is, alternate growth–decay of the Rh_2 band following 297-nm atomic irradiation with a gradual and overall intensity loss of Rh and Rh_2 species. The latter two species are both slowly channelled into Rh_3 and higher clusters which are themselves overlapped by Rh and Rh_2 bands, as suggested in the previous section. Assignment of an underlying 297-nm Rh_2 band can easily be fitted into the Norman $X\alpha$ Rh_2 calculated scheme described earlier (Table V).

Possible Relevance of the Optical Properties of Very Small Naked Cobalt and Rhodium Clusters to the Problem of Characterizing the Same Clusters Attached to Solid Supports

In this concluding section we will briefly consider the effect of the anchoring groups of solid supports on the spectroscopic properties of immobilized metal clusters. At the outset, one cannot overemphasize the importance of understanding the perturbing effects of "strong and weak" matrix environments on cluster electronic/structural properties; these are central to the problem of unravelling the size and support dependence of catalytic and chemisorptive behavior of metal particles as well as for actually characterizing the nuclearity of the attached clusters themselves.

Clearly a number of experimental and theoretical techniques can be brought to bear on the question of the structure of an attached metal cluster. These include EXAFS methods which have recently provided the structure of, for example, the polymer-bound analogue of Wilkinson's catalyst[28] and an insight into the interatomic distances and coordination geometries of SiO_2-supported Pt and Ru/Cu metal clusters.[29] Electron microscopy, for cluster systems larger than about 10 Å, is also proving valuable for determining the geometrical structure of supported clusters as seen from the recent discovery of two-dimensional raft and three-dimensional particle arrays for Ru/SiO_2 and $Ru/Cu/SiO_2$ clusters.[30] Laser Raman spectroscopic studies aimed at detecting metal–metal bonds may also prove useful for elucidating the structures of clusters attached to solid supports as well as clusters entrapped within the confines of weakly interacting matrices.[31]

As mentioned earlier, once a carbonyl cluster precursor is incorporated into the reaction cycle of adsorption, thermal decarbonylation and reduction, infrared methods can easily discern whether ligand detachment from the original cluster core is complete; however, only by reversible ligand-association studies can one infer that a very small size of particle has been retained on the support indicative of low aggregation.[1] If the carbonyl portion of an anchored, regenerated carbonyl cluster complex closely resembles that of the originally attached complex (for convincing examples of this see ref 1d–f), one can feel reasonably secure that the integrity of the cluster framework has been maintained throughout the adsorption, ligand dissociation, catalytic testing, and regeneration procedures. On the other hand, if, during these events, the removal of surface stabilizing ligands or the presence of weak surface-cluster interactions allows unrestricted metal migration on the solid support, cluster agglomeration will ensue to the point of coordination saturation via metal–metal bond formation. This can be seen either by the physical appearance of metal particles on the support as monitored by electron microscopy,[1d] by the transformation of the carbonyl region of the IR spectrum of the original cluster complex to one resembling CO chemisorbed on the bulk metal,[1d-f] or by the changes in the kinetic characteristics of a test catalytic reaction.[1d]

In this discussion, we address the idea of employing optical spectroscopy for directly probing the metal framework of an attached cluster both in the presence and absence of cluster and surface ligands. As a reference point for the truly naked-cluster optical data, one would ideally require gas-phase measurements; however, these are generally unavailable for the transition metals, and it is our contention that matrix optical data for small, well-defined M_n systems[15] can adequately serve this purpose. In the context of the present study, we note with special interest the *remarkable similarity* between the optical absorption spectra (200–700 nm) of Ag_n clusters ($1 < n < 7$) entrapped within the lattice confines of weakly interacting inert gas,[15d,40] alkane and high-molecular-weight wax matrices,[33c] and quench-condensed ice films,[33c] and within the pores of vacuum-dehydrated, silver-exchanged zeolite-Y.[39] In addition, the close correspondence between the fluorescence emission of 300–330-nm excited Ag atoms in inert gas[33a,41,42] and zeolite[39] supports is most striking. Aside from inhomogeneous band-broadening effects, the *minor* perturbation of the excitation energies of small Ag_n aggregates by the neighboring oxide ions of the encapsulating zeolite framework from that of a "pseudo-gas-phase" environment points to a *weak metal–support interaction* in this particular system.

Over the past few years a fair number of optical studies have been reported for $M_2(CO)_l$, $M_3(CO)_m$ and $M_4(CO)_n$ coordinatively saturated carbonyl cluster systems of the Mn, Fe, and Co groups of metals.[32] Such studies have usually been directed at the *lowest energy electronic excitations* characteristic of the metal cluster chromophores. Most prominent among these investigations has been the identification of metal-localized transitions from σ bonding to σ antibonding molecular orbitals.[32] Depopulation of the bonding molecular orbitals has been shown to dictate the photochemistry of these compounds by inducing homolytic cleavage of the metal–metal bond(s).[32] Photofragmentation of metal carbonyl clusters has been reported to occur in a number of instances, and com-

Table VI. Localized Metal-Metal Optical Transitions[b] for $M_{2,3}$, $M_2(CO)_8$, and $M_4(CO)_{12}$ (M = Co, Rh)

$Co_n(CO)_m$	nm	$Rh_n(CO)_m$	nm
Co_2	418,[a] 442	Rh_2	400,[a] 460
Co_3	400–480[a]	Rh_3	490[a]
		Rh_n	560[a]
$Co_2(CO)_8$ [32]	282[c]	$Rh_2(CO)_8$ [35]	260
$Co_4(CO)_{12}$ [32]	370	$Rh_4(CO)_{12}$ [32]	300

[a] Very weak bands; assignments tentative. [b] Associated with mainly localized σ–σ^* types of transitions (see also ref 43). [c] Bridge-bonded isomer. The corresponding excitation for the nonbridged isomer occurs at 370 nm.

plementary electronic spectral studies have greatly aided the interpretation of the photochemistry.[32] In this context it is pertinent to note that photoisomerizations and photofragmentations of naked-cluster systems entrapped within low-temperature, weakly interacting matrices have also been recorded and probed by UV–visible absorption[33a,b] and emission[41] spectroscopy.

Within the framework of the present discussion, which focusses on the nature and magnitude of the perturbation of very small Co- and Rh-cluster electronic and optical properties by discrete ligands, with a natural extension to similar ligands appended to solid supports, it is interesting to compare the optical spectra of $Co_2(CO)_8$, $Co_4(CO)_{12}$, $Rh_2(CO)_8$, and $Rh_4(CO)_{12}$[32] with those recorded for $Co_{2,3}$ and $Rh_{2,3}$. (It is worth noting here that an SCF–Xα–SW–MO approach to this type of problem, within a localized bonding approximation, has been reported for Pt/SiO_2 and Ru/SiO_2 clusters by Johnson and co-workers.[34])

As one would anticipate that transition metal–metal localized excitations might be sensitive to cluster attachment to a solid support, let us survey the available optical data for the cobalt and rhodium naked clusters and carbonyl complexes listed in Table VI in an attempt to discover trends that might assist in the determination of the nuclearity of immobilized metal-cluster systems.

Realizing that there exists some degree of uncertainty regarding cluster structure and optical assignments,[43] one can nevertheless deduce from Table VI that (a) bridging CO has the effect of *blue*-shifting metal-localized σ–σ^* transitions with respect to the corresponding nonbridged situation (metal–metal proximity, orbital-overlap effects), (b) increasing metal atomic weight within a group has the effect of *blue*-shifting localized metal–metal excitations (increasing overlap between larger orbitals and causing greater separation of bonding and antibonding levels), (c) increasing metal nuclearity has the effect of *red*-shifting localized metal excitations (decreasing HOMO–LUMO band gap with buildup of metal-localized molecular orbitals), (d) carbonyl complexation to the naked metal cluster has the effect of *blue*-shifting metal-localized excitations (combination of stabilization and destabilizing influences on metal bonding and antibonding molecular orbitals).

Most of these observations can be rationalized on the basis of simple framework molecular orbital arguments[36] involving metal-localized molecular orbitals. *Particularly striking, however, are the marked effects of carbonyl complexation (Table VI) on the assigned metal-localized transitions.*[43] (Along these lines we note also that previous work on di-, tri-, and tetranuclear metal carbonyl clusters has shown that the energy of σ–σ^*-localized transitions is affected by phosphine substitution in a somewhat unpredictable manner, emphasizing that several electronic effects control the energy of these σ–σ^* excitations.[32])

A cautious statement at this stage of the research would be that one can expect a sizable perturbation of the metal valence energy levels of a small, naked cluster when attached to strongly interacting surface ligands or active surface groups of functionalized polymers or oxide supports. Even so, it would seem that the opportunity exists of being able to assess the importance of cluster-support effects, to characterize metal-cluster structure and nuclearity from the optical data of immobilized metal clusters[15d,33c,39,40] and/or to decide whether or not metal-cluster size has been altered during adsorption and vacuum-thermal decarbonylation of a cluster carbonyl complex simply from comparisons of naked-cluster optical properties with the corresponding data of the anchored cluster cores. Future experimental and theoretical studies should help clarify these intriguing propositions.

Acknowledgment. We acknowledge the financial assistance of the National Research Council of Canada's Operating, New Ideas, and Strategic Energy Grants Programs, Imperial Oil of Canada, the Connaught Foundation, Erindale College, and the Lash Miller Chemical Laboratories. A.J.L.H. also expresses her gratitude to the NRCC for a scholarship throughout the tenure of her graduate research. Stimulating and helpful correspondence with Dr. Joe Norman, Jr., during the writing of this paper is gratefully appreciated. Valuable discussions concerning the preliminary Xα results of Mr. Steven Mitchell, Mr. Douglas McIntosh, and Dr. Richard Messmer are also recognized.

Registry No. Co, 7440-48-4; Rh, 7440-16-6; Co_2, 37210-16-5; Rh_2, 12596-98-4; Co_3, 70084-46-7; Rh_3, 70084-47-8.

References and Notes

(1) (a) M. Ichikawa, *J. Chem. Soc., Chem. Commun.*, **11**, 26 (1976); (b) H. Conrad, G. Ertl, H. Knozinger, J. Kuppers, and E. E. Latta, *Chem. Phys. Lett.*, **42**, 155 (1976); W. Plummer, private communication; (c) J. P. Collman, L. S. Hegedus, M. P. Cooke, J. R. Norton, G. Dolcetti, and D. N. Marquardt, *J. Am. Chem. Soc.*, **94**, 789 (1972); (d) M. S. Jarrell, B. C. Gates, and E. D. Nicholson, *ibid.*, **100**, 5727 (1978); (e) J. L. Bilhon, V. Bilhon-Bonguol, W. F. Graydon, J. M. Bassett, A. K. Smith, G. M. Zanderighi, and R. Ugo, *J. Organomet. Chem.*, **153**, 73 (1978); (f) J. J. Rafalko, J. Lieto, B. C. Gates, and G. L. Schrader, Jr., *J. Chem. Soc., Chem. Commun.*, 540 (1978); (g) H. D. Kaesz, R. A. Love, B. A. Matrana, A. P. Humphries, and S. Siegel, paper presented before the Petroleum Division, 174th National Meeting of the American Chemical Society, Chicago, IL, 1977; (h) J. R. Anderson, P. S. Elmes, R. F. Howe, and R. E. Mainwaring, *J. Catal.*, **50**, 508 (1977), and references cited therein.
(2) G. A. Mills and F. W. Steffgen, *Catal. Rev.*, **8**, 159 (1973), and references therein.
(3) (a) M. A. Vannice, *Catal. Rev.*, **14**, 153 (1976), and references therein; (b) G. Henrici-Olivé and S. Olivé, *Angew. Chem., Int. Ed. Engl.*, **15**, 136 (1976), and references therein.
(4) E. Papirer, *C. R. Hebd. Seances Acad. Sci., Ser. A*, **285**, 73 (1977).
(5) R. D. Rieke, *Acc. Chem. Res.*, **10**, 301 (1977).
(6) H. B. Gray and C. C. Frazier, private communication.
(7) K. Klabunde, private communication.
(8) W. Wada, *J. Phys. (Paris)*, C2, 219 (1977).
(9) D. M. Mann and H. P. Broida, *J. Chem. Phys.*, **55**, 84 (1961).
(10) D. H. W. Carstens, W. Brashear, D. E. Eslinger, and D. M. Gruen, *Appl. Spectrosc.*, **26**, 184 (1972).
(11) (a) C. E. Moore, *Natl. Bur. Stand. (U.S.) Circ.*, No. 467, **1** (1949); **2** (1952); **3** (1958); (b) C. H. Corliss and W. L. Bozman, *Natl. Bur. Stand. Monogr.*, No. **53** (1962).
(12) D. M. Gruen and D. H. W. Carstens, *J. Chem. Phys.*, **54**, 5206 (1971).
(13) A. Kant and B. Strauss, *J. Chem. Phys.*, **41**, 3806 (1964).
(14) W. F. Cooper, G. A. Clarke, and C. R. Hare, *J. Phys. Chem.*, **76**, 2268 (1972).
(15) (a) E. P. Kundig, M. Moskovits, and G. A. Ozin, *Nature (London)*, **254**, 503 (1975); (b) T. C. DeVore, A. Ewing, H. F. Franzen, and V. Calder, *Chem. Phys. Lett.*, **35**, 78 (1975); (c) H. Huber, E. P. Kundig, M. Moskovits, and G. A. Ozin, *J. Am. Chem. Soc.*, **97**, 2097 (1975); (d) H. Huber and G. A. Ozin, *Inorg. Chem.*, **17**, 155 (1978); (e) J. E. Hulse and M. Moskovits, *J. Chem. Phys.*, **66**, 3988 (1977); (f) W. Klotzbucher and G. A. Ozin, *J. Mol. Catal.*, **3**, 195 (1977); (g) M. Moskovits and J. E. Hulse, *J. Chem. Phys.*, **67**, 4271 (1977), and references therein.
(16) M. Moskovits and J. E. Hulse, *J. Chem. Soc., Faraday Trans. 2*, **73**, 471 (1977).
(17) S. A. Mitchell, D. F. McIntosh, R. P. Messmer, G. A. Ozin, unpublished results.
(18) M. Belzons and G. Rasigni, *C. R. Hebd. Seances Acad. Sci.*, **261**, 4042 (1965); M. Belzons, *ibid.*, **260**, 4707 (1965).
(19) G. A. Ozin and A. Vander Voet, *Can. J. Chem.*, **51**, 3332 (1973).
(20) A. J. L. Hanlan and G. A. Ozin, *J. Am. Chem. Soc.*, **96**, 6324 (1974).
(21) A. J. L. Hanlan and G. A. Ozin, *Inorg. Chem.*, **16**, 2858 (1977).
(22) A. J. L. Hanlan and G. A. Ozin, *Inorg. Chem.*, **16**, 2848 (1977).

(23) (a) N. W. Cant and W. K. Hall, *J. Catal.*, **16**, 220 (1970); (b) N. W. Cant and W. K. Hall, *ibid.*, **27**, 70 (1972), and references therein.
(24) J. C. Schlatter and K. C. Taylor, *J. Catal.*, **49**, 42 (1977).
(25) N. Rösch and D. Menzel, *Chem. Phys.*, **13**, 243 (1976); G. A. Ozin, D. McIntosh, S. Mitchell, and R. P. Messmer, Ag_n SCF–Xα–SW calculations, to be published.
(26) G. C. Smith, T. P. Chojnacki, S. R. Dasgupta, K. Iwatate, and K. L. Watters, *Inorg. Chem.*, **14**, 1419 (1975).
(27) J. G. Norman and H. J. Kolari, *J. Am. Chem. Soc.*, **100**, 791 (1978).
(28) J. Reed, P. Eisenberger, B. K. Teo, and B. M. Kincaid, *J. Am. Chem. Soc.*, **99**, 5217 (1977).
(29) F. W. Lytle, G. H. Via, and J. H. Sinfelt, *J. Chem. Phys.*, **67**, 3831 (1977); **68**, 2009 (1978).
(30) E. B. Prestridge, G. H. Via, and J. H. Sinfelt, *J. Catal.*, **50**, 115 (1977).
(31) (a) H. U. Becker, K. Manzel, R. Minkwitz, and W. Schulze, *Chem. Phys. Lett.*, **55**, 59 (1978); (b) A. Givan and A. Loewenschuss, *J. Chem. Phys.*, **69**, 1790 (1978).
(32) (a) R. A. Levenson and H. B. Gray, *J. Am. Chem. Soc.*, **97**, 6042 (1975); (b) M. S. Wrighton, *Top. Curr. Chem.*, **65**, 37 (1975); (c) D. R. Tyler, and H. B. Gray, private communication, California Institute of Technology, 1977; (d) H. B. Abrahamson, C. C. Frazier, D. S. Ginley, H. B. Gray, J. Lilliethal, D. R. Tyler, and M. S. Wrighton, *Inorg. Chem.*, **16**, 1554 (1977); (e) B. F. G. Johnson, J. Lewis, and M. V. Twigg, *J. Organomet. Chem.*, **67**, C76 (1974); (f) R. G. Austin, R. S. Paonessa, and M. S. Wrighton, 174th National Meeting of the American Chemical Society, Chicago, IL, 1977, INOR 161; G. L. Geoffroy and R. A. Epstein, *ibid.*, INOR 158.
(33) (a) G. A. Ozin, S. Mitchell, J. G. Norman, Jr., and L. Noodleman, *J. Am. Chem. Soc.*, in press; (b) G. A. Ozin, H. Huber, and S. Mitchell, *Inorg. Chem.*, in press; the disilver and trisilver naked cluster cryophotochemistry paper was first presented by G. A. Ozin at the American Chemical Society Metal Cluster Symposium, Anaheim, CA, March 1978. (c) G. A. Ozin, S. Mitchell, H. Huber, and P. McKenzie, submitted for publication in *Inorg. Chem.*
(34) K. H. Johnson, A. C. Balazs, and H. J. Kolari, *Surf. Sci.*, **72**, 733 (1978).
(35) H. B. Gray, A. J. L. Hanlan, and G. A. Ozin, *Inorg. Chem.*, in press.
(36) M. Elian and R. Hoffmann, *Inorg. Chem.*, **14**, 1058 (1975).
(37) E. P. Kundig, M. Moskovits, and G. A. Ozin, *J. Mol. Struct.*, **14**, 137 (1972).
(38) M. Moskovits and G. A. Ozin, *Appl. Spectrosc.*, **26**, 487 (1972).
(39) R. Kellerman and J. Texter, personal communication; Xerox Corp. Report; *J. Chem. Phys.*, **70**, 1562 (1979).
(40) W. Schulze, H. U. Becker, and D. Leutloff, *J. Phys. (Paris), Colloq.*, 7 (1977); W. Schulze, H. U. Becker, and H. Abe, *Ber. Bunsenges Phys. Chem.*, **82**, 138 (1978); *Chem. Phys.*, **35**, 177 (1978).
(41) G. A. Ozin, G. Kenney-Wallace, S. Mitchell, J. Farrel, and H. Huber, paper presented by G. A. Ozin at the Materials Science Cluster Symposium, Boston, MA, April 1978 (to be published).
(42) D. M. Kolb and D. Leutloff, *Chem. Phys. Lett.*, **55**, 264 (1978).
(43) Dr. Joe Norman, Jr. (private communication), has suggested that the sensitivity of the minimum-energy-cluster electronic configuration to spin-polarization effects (vis-ā-vis Rh_2 SCF–Xα–SW calculations[27]) could favor the nearby $2\sigma_g^1 1\pi_g^2 1\sigma_u^1$ state over our preliminary Xα spin-restricted $2\sigma_g^2 1\pi_g^2 1\sigma_u^0$ ground state. Moreover, qualitative oscillator strength arguments (based on Cu_2,Ag_2 computations[33a]) imply that a *blue shift* of the entire calculated optical spectrum by about 7000 cm^{-1} (corresponding to shorter Co–Co and Rh–Rh distances of 2.0 and 2.2 Å, respectively; cf. the 2.32- and 2.39-Å metal–metal bond lengths employed in the existing SCF–Xα–SW calculations) would necessitate a reassignment of the most prominent bands of Co_2 and Rh_2 (270–350 nm) to $2\sigma_g \rightarrow 2\pi_u$ and $1,2\sigma_g \rightarrow 1,2\sigma_u$ excitations. In this case, cluster-support interactions may not be quite as pronounced as our discussion of the data presented in Table VI leads one to believe (see the last section of this paper).
(44) Although a one-electron transition for Rh_2 at 344 nm will only reduce the formal bond order from 2 to 1 (according to the assignments of Table V and Figure 9), excitation at 344 nm provides more than enough energy to photodissociate the Rh–Rh bond, especially in a rare gas matrix environment. (The bond dissociation energy of the Rh_2 molecule has been estimated from high-temperature Knudsen cell effusion-mass spectrometric data to be 67 kcal/mol: D. L. Cocke and G. A. Gingerich, *J. Chem. Phys.* **60**, 1958 (1974).) One must also be alert to the fact that the uncertainty in determining the extent of orbital contributions to the Rh–Rh bond from Xα methods may make it impractical to assign a formal bond order to Rh_2.

Contribution from Lash Miller Chemical Laboratories and Erindale College, University of Toronto, Toronto, Ontario, Canada, and Contribution No. 6027 from the Arthur Amos Noyes Laboratory, California Institute of Technology, Pasadena, California 91125

An Electronic Spectroscopic Study of Bridge-Bonded Dirhodium Octacarbonyl

A. J. LEE HANLAN, GEOFFREY A. OZIN,* and HARRY B. GRAY

Received January 19, 1979

The thermally induced (15–35 K) dimerization reaction of the 17-electron species $Rh(CO)_4$ (synthesized from Rh/CO $\simeq 1/10^4$; 15 K matrix cocondensations) to the bridge-bonded form of $Rh_2(CO)_8$, originally detected by matrix infrared spectroscopy, has now been monitored by electronic absorption spectroscopy. In this way the electronic spectrum of $Rh_2(CO)_8$ is defined and compared with corresponding spectroscopic data for the bridge-bonded form of $Co_2(CO)_8$. An intense band in the spectrum of $Rh_2(CO)_8$ at 260 nm is assigned to a $\sigma \rightarrow \sigma^*$ transition, whereas a strong MLCT absorption system is observed at about 225 nm. The $Rh_2(CO)_8$ $\sigma \rightarrow \sigma^*$ transition is blue-shifted from that found in $Co_2(CO)_8$ (282 nm), as expected.

Introduction

Considerable work has been undertaken to understand the electronic spectra of metal–metal-bonded $M_2(CO)_n$ and $M_2(CO)_nL_m$ complexes.[1] On the other hand, very little has appeared concerning binuclear metal carbonyl complexes that contain bridging carbonyl moieties. Recently Gray published[1b] an interpretation of the electronic spectra of $Co_2(CO)_8$ in both the nonbridged and CO-bridged isomeric forms. A $\sigma \rightarrow \sigma^*$ absorption system was identified in the spectrum of each isomer, although the assignment in the case of the bridge-bonded molecule was not as clear-cut as it was for nonbridged $Co_2(CO)_8$.

In an earlier publication we described[2] the synthesis and characterization of $Rh_2(CO)_8$ by Rh-atom cryochemical techniques in conjunction with matrix-isolation infrared spectroscopy. The dimer was identified by Rh concentration and matrix-annealing experiments and was found to exist exclusively in the bridge-bonded form.[3] We have now measured the electronic spectrum of $Rh_2(CO)_8$, and comparisons with data collected previously for $Rh(CO)_4$,[4] $Co(CO)_4$,[4] and bridge-bonded $Co_2(CO)_8$[1b] have allowed us to assign the two most intense ultraviolet features.

* To whom correspondence should be addressed at Lash Miller Chemical Laboratories.

Experimental Section

Through use of Rh/CO $\simeq 1/10^4$ and 15 K deposition conditions, the electronic absorption spectra consist primarily of $Rh(CO)_4$ as seen through the eye of the corresponding infrared experiment,[2] recorded on the same sample. Temperature-programmed annealing experiments in the range 15–35 K induce decay of all of the absorptions associated with $Rh(CO)_4$, with accompanying growth of several new absorptions attributable to $Rh_2(CO)_8$.[2] Rhodium metal was supplied by A. D. MacKay, New York, and research grade $^{12}C^{16}O$ (99.999%) by Matheson of Canada. Rh/CO matrices were deposited on a NaCl optical window cooled to 15 K by an Air Products Displex closed-cycle helium refrigerator. Absorption spectra were recorded on a Varian Techtron 635 UV–visible spectrophotometer.

0020-1669/79/1318-1790$01.00/0